DOI: 10.1002/cbic.200800796

Off-Target Decoding of a Multitarget Kinase Inhibitor by Chemical Proteomics

Enrico Missner,*[a, b] Inke Bahr,[a] Volker Badock,[a] Ulrich Lücking,[a] Gerhard Siemeister,[a] and Peter Donner[a]

Since the approval of the first selective tyrosine kinase inhibitor, imatinib, various drugs have been developed to target protein kinases. However, due to a high degree of structural conservation of the ATP binding site, off-target effects have been reported for several drugs. Here, we report on off-target decoding for a multitarget protein kinase inhibitor by chemical proteomics, by focusing on interactions with nonprotein kinases. We tested two different routes for the immobilization of the inhibitor on a carrier matrix, and thus identified off-targets that interact with distinct compound moieties. Besides several of the kinases known to bind to the compound, the pyridoxal kinase (PDXK), which has been described to interact with the CDK inhibitor (*R*)-roscovitine, was captured. The PDXK–inhibitor interaction was shown to occur at the substrate binding site rather than at the ATP binding site. In addition, carbonic anhydrase 2 (CA2) binding was demonstrated, and the determination of the IC_{50} revealed an enzyme inhibition in the submicromolar range. The data demonstrate that different compound immobilization routes for chemical proteomics approaches are a valuable method to improve the knowledge about the off-target profile of a compound.

Introduction

Protein kinases play a central role in many cellular processes like metabolism, transcription, cell cycle progression, cytoskeletal rearrangement and cell movement, apoptosis, and differentiation.[1] Thus, the deregulation of kinase activities can lead to various severe pathological conditions,[2] for example, cancer,[3–9] central nervous system disorders,[10,11] autoimmune disease,[12] post-transplant immunosuppression,[13] osteoporosis,[14] and metabolic disorders.[15] A variety of studies show that kinases are suitable targets for the treatment of the diseases that are caused by such deregulation. The approval of the first selective tyrosine kinase inhibitor imatinib (Gleevec®) has extremely encouraged the pharma industry to generate a multitude of kinase inhibitors.[16]

In the majority of current drug discovery strategies, libraries of compounds are screened at an early stage against recombinant, isolated, purified proteins or functional protein domains. Initially identified hits are further optimized in regard to their potency. Compound selectivity is then addressed by counter-screens in protein kinase assay panels; this results in a small number of lead compounds.[17–19] However, besides the on-target kinase inhibition, the compounds might affect multiple unknown- and off-targets, which either contribute to the biological effect of the kinase inhibitor or that counteract or lead to detrimental side-effects. Indeed, due to a high degree of structural conservation of the ATP binding site, toward which most inhibitors are directed, multiple targets and off-target effects, which contribute to the biological activity, have been reported for several drugs.[20–24] To obtain deeper insights into the target space of a compound, additional strategies for a more global compound profiling have been developed, such as chemical proteomics.[25–28]

Chemical proteomics has been successfully implemented to directly obtain protein-binding profiles of compounds from cell lysates. For affinity pull-downs of drug targets in an unbiased fashion, a small-molecule ligand is modified by introducing a suitable linker; this enables immobilization on a solid support (referred to as matrix). Subsequently, the compound matrix is incubated with a protein extract, and captured proteins are analyzed by mass spectrometry or immunodetection (Figure S1 in the Supporting Information). The Kinobeads™ approach is an advanced technology that quantitatively measures the competition of a free compound with an affinity matrix consisting of several immobilized tool compounds selected to capture a large portion of the expressed kinome.[20,29] However, by profiling compounds against a subset of proteins captured by tool compounds, the unbiased character in regard to potential off-targets, which is a particular advantage of chemical proteomics, partly gets lost. In fact, an unbiased off-target characterization during the lead optimization processes is highly desirable for gaining deeper insights into the biological activity and off-target profile of a drug.

[a] *E. Missner, Dr. I. Bahr, Dr. V. Badock, Dr. U. Lücking, Dr. G. Siemeister, Prof. P. Donner*
Bayer Schering Pharma AG, Global Drug Discovery
13342 Berlin (Germany)
Fax: (+49)30-468-16707
E-mail: enrico.missner@bayerhealthcare.com

[b] *E. Missner*
Institute for Chemistry and Biochemistry, FU Berlin
Thielallee 63, 14195 Berlin (Germany)

Supporting information for this article is available on the WWW under http://dx.doi.org/10.1002/cbic.200800796.

Recently, the binding profile of (*R*)-roscovitine (CYC202), a CDK inhibitor that is currently in phase 2 clinical trials for various cancer indications,[30,31] was investigated by affinity chromatography with the drug immobilized on a sepharose matrix.[32,33] In addition to the expected targets extracellular signal-regulated kinase 1 (ERK1), ERK2, and cyclin-dependent kinases (CDKs), the previously unknown off-target, pyridoxal kinase, was identified. This nonprotein kinase is responsible for the phosphorylation of pyridoxal (PL), pyridoxine (PN) and pyridoxamine (PM) to the respective 5′-phosphate esters PLP, PNP, and PMP, which are the active forms of vitamin B6. Vitamin B6 is a cofactor for numerous enzymes, such as aminotransferases and decarboxylases, of which many are involved in amino acid and neurotransmitter metabolism.[34–36] Low levels of PLP, which is caused by a down-regulation of brain PDXK expression or by PL competitors, are correlated with epilepsy in animal models.[37,38] It has been suggested that the unexpected binding activity of (*R*)-roscovitine to PDXK explains some of the biological effects of the drug or dilutes its on-target effects by reducing the amount of free (*R*)-roscovitine that is available for the desired target interaction.

Herein, we report on the results of a chemical proteomics based, unbiased off-target decoding approach for a small-molecule ATP-competitive multitarget protein kinase inhibitor (C1). This inhibitor was previously shown to have high potency against CDK2, and macrocyclic derivatives were described as multitarget CDK and VEGF-R inhibitors with potent antiproliferative activities towards various human tumor cells and in a human tumor xenograft model.[39] Based on a computational model of a compound–target complex, we carried out two different immobilization routes that were aimed at uncovering potential off-targets that interact with distinct compound moieties. Furthermore, we generated a soluble mimic of the immobilized inhibitor to confirm that immobilization of the compound does not interfere with its functionality. Additionally, potential linker effects caused by the immobilization method could be analyzed. During our studies, we found that pyridoxal kinase (PDXK), which is a recently described off-target for (*R*)-roscovitine, and carbonic anhydrase 2 (CA2) bind to the immobilized inhibitor. We identified the targeted binding site of PDXK, and quantitatively analyzed the binding of the compound to recombinant PDXK and CA2. Altogether, we not only improved our knowledge about the off-target profile of our inhibitor, but also introduced the utilization of different compound immobilization routes as a valuable method for a more comprehensive off-target profiling by chemical proteomics.

Results and Discussion

Immobilization of the inhibitor C1 at the sulfonamide moiety preserves its functionality

A computational model of the protein kinase inhibitor C1 in complex with its target protein, CDK2, was derived from co-crystallization experiments of CDK2 in complex with various C1 analogues.[39] Due to the solvent accessibility of the sulfonamide moiety of C1, this group was identified as an appropriate site for compound immobilization in a chemical proteomics approach (Figure 1). After introducing a short linker at the sulfonamide group to give C1–SL, we immobilized this short-

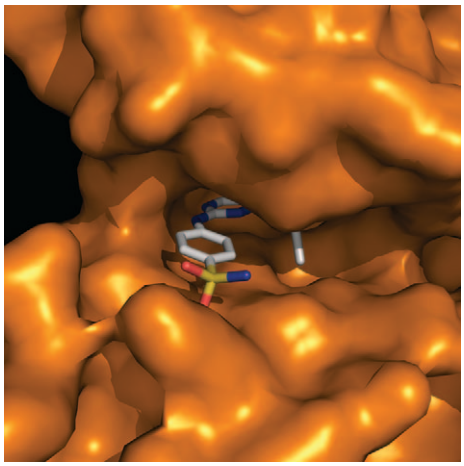

Figure 1. Computational model of C1 in complex with the ATP binding pocket of CDK2. Due to its solvent accessibility, the sulfonamide group was identified as an appropriate site for a functional linker attachment; this gave C1–SL.

linker analogue to a solid support and thereby generated a C1–matrix (Scheme 1). Additionally, a soluble mimic of the compound matrix was synthesized to confirm that immobilization via the sulfonamide does not interfere with the functionality of the compound. For this purpose, C1 was provided with a linker that was similar to the linking structure of the sepharose matrix, to give the long-linker analogue C1–LL, which is referred to as "mimic".

The IC_{50} determinations for C1, C1–SL and the mimic revealed that they all inhibit CDK2/CycE in the low-nanomolar range (Table 1). Because the mimic (C1–LL) showed a high inhibitory potential against CDK2/CycE, we concluded that the C1 matrix is suitable for the affinity enrichment of binders. The in vitro affinity capturing experiments were performed by using HeLa cell extracts, and the binding of CDK2 to the C1 matrix was confirmed by immunoblotting (Figure 2A).

Table 1. Structure–activity relationship observations for C1 analogues.

Compound	C1	C1–SL	mimic (C1–LL)	C1a
IC_{50} [nM] CDK2/CycE[a]	1	1	3	18

[a] HTRF®: homogeneous time resolved fluorescence assay.

For the identification of a suitable elution buffer, the captured CDK2 was sequentially eluted by applying an ATP/$MgCl_2$ buffer, followed by a saturated C1–SL solution (approximately 150 μM) and finally LDS-sample buffer (LDS-SB) and heat. Neither ATP nor compound buffer was found to quantitatively elute CDK2 from the matrix. We assumed that the high local

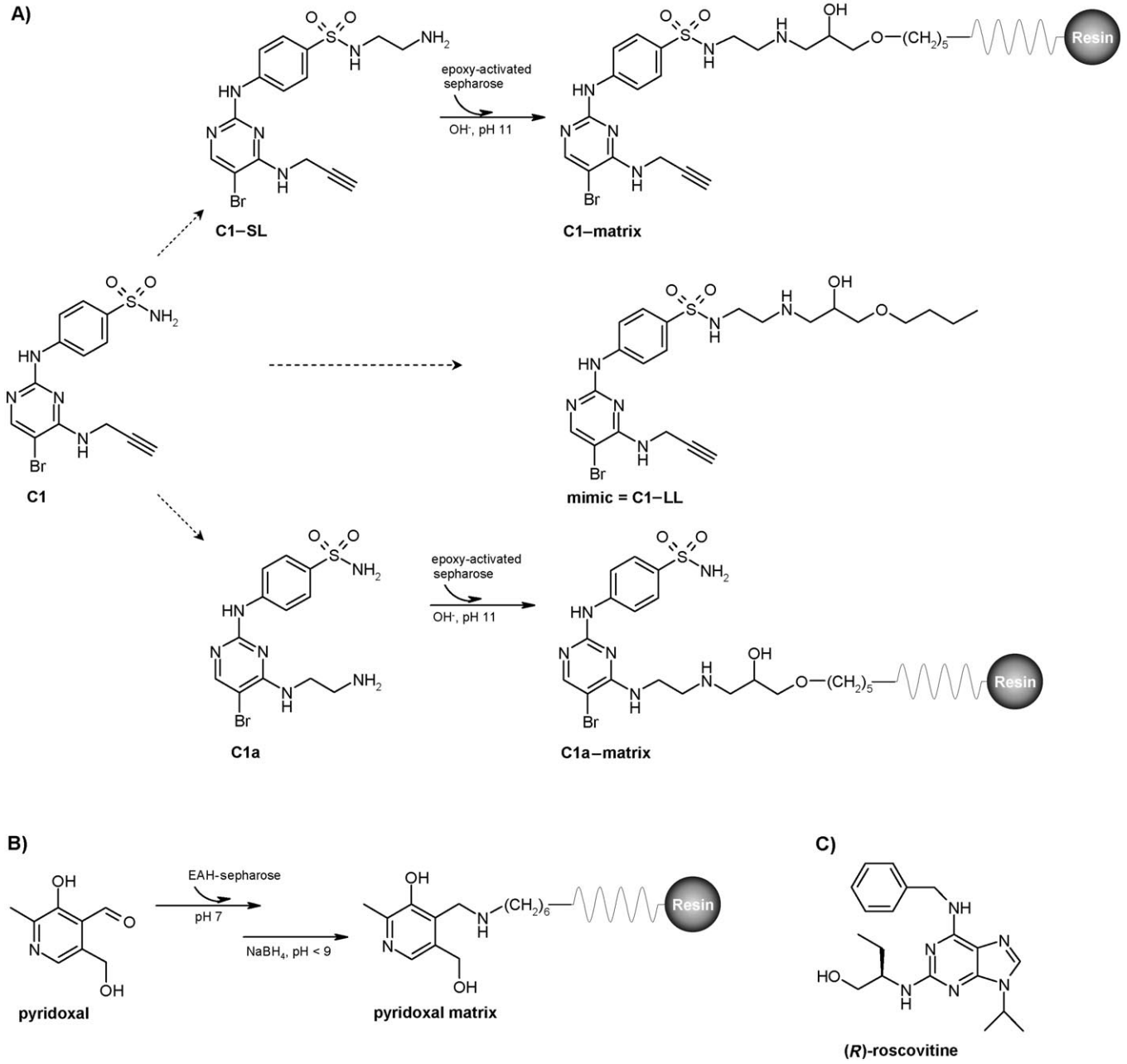

Scheme 1. Generation of affinity matrices. A) Based on computational modeling of C1 in complex with CDK2, the "short linker" analogue, C1–SL, was generated and coupled to epoxy-activated Sepharose™ beads. The resulting C1 matrix was used for affinity purification of binders in a chemical proteomics approach. Furthermore, a soluble mimic of the immobilized inhibitor, referred to as C1–LL (C1–"long-linker") or mimic, was generated to confirm suitable compound immobilization in regard to target protein binding. Additionally, the mimic was used to analyze potential effects of the linker. For an alternative immobilization route, the C1 analogue, C1a, was immobilized to epoxy-activated Sepharose™ beads at the 4-position; this resulted in the C1a–matrix. This affinity matrix was used to capture proteins that interacted through the sulfonamide moiety. B) The substrate of PDXK, pyridoxal, was coupled to EAH–Sepharose™ in a two-step reaction. The resulting pyridoxal matrix was employed for the characterization of the PDXK–C1 interaction and for the purification of recombinant PDXK. C) The purine class CDK inhibitor, (*R*)-roscovitine (CYC202).

compound concentration on the bead surface and the limited solubility of the free compound prevented CDK2 from being quantitatively eluted by ATP or free compound. Thus, unless otherwise stated, we applied denaturing conditions by boiling beads in LDS-SB for subsequent experiments for a complete but unspecific elution of the captured proteins.

The protein-binding profile of C1 matrix

After having demonstrated the suitability of the C1 matrix for capturing CDK2, we employed LC-MS/MS analysis of eluted proteins by using HeLa cell extracts to obtain a protein-binding profile for the C1 matrix (Figure 2B). The overlap of two independent experiments when using compound matrix resulted in the identification of 150 proteins that fulfill the accept-

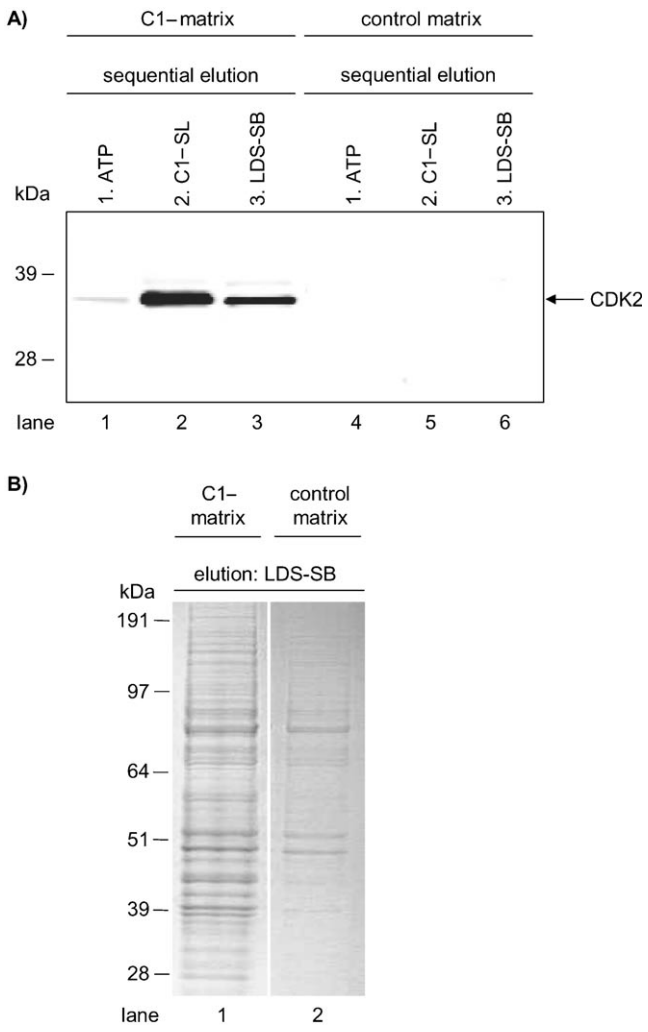

Figure 2. A) Proof-of-concept: HeLa cell extracts were incubated with compound matrix and control matrix. After several washing steps, captured proteins were eluted sequentially with: 1) ATP (10 mM)/$MgCl_2$ (10 mM)/low-salt washing buffer (detailed in the Experimental Section); 2) a saturated C1–SL solution in low-salt washing buffer; 3) 2× LDS-SB/heat. CDK2 binding to C1 matrix was demonstrated by immunodetection (lanes 1–3). No CDK2 enrichment resulted with the control matrix (lanes 4–6). B) Affinity pull-down by using C1 matrix: HeLa cell extracts were loaded on C1 and control matrix. After extensive washing, bound proteins were eluted by boiling the beads in 2× LDS-SB and analyzed by SDS-PAGE, Coomassie staining and LC–MS/MS.

prehensive interaction profile for the C1 matrix, more cell lines have to be screened.

C1: high potency, poor selectivity

C1 has been optimized in regard to potent inhibition of CDK2. However, its selectivity was barely improved and is considered to be poor. Testing of C1 against the 27 protein kinases that were identified in our chemical proteomics experiments revealed its limited selectivity (Figure 3). At a concentration of 1 μM, C1 inhibited three other CDKs (CDK1, -5, and -9) by more

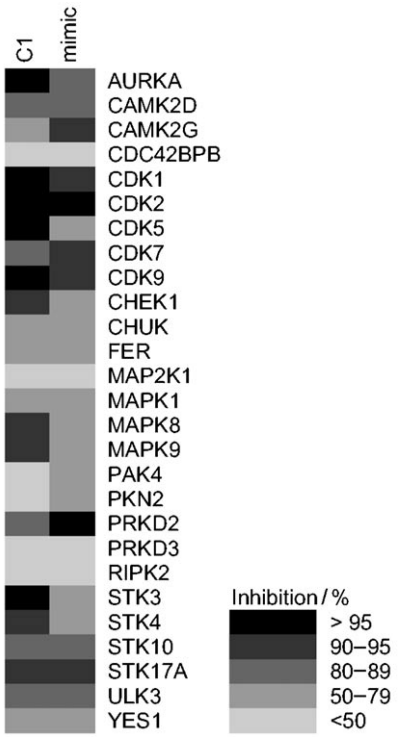

Figure 3. Percentage inhibition of 27 protein kinases identified by affinity pull-down experiments with C1 and mimic (C1–LL). Inhibitors were tested at 1 μM compound and 10 μM ATP. Only a subset of protein kinases captured by the C1 matrix, were strongly inhibited by C1. Comparison of the selectivity patterns of C1 and the mimic revealed moderate effects of the linker on the inhibitory potential. Data were obtained from the Upstate–Millipore KinaseProfiler™ service.

ance criteria described in the Experimental Section (Table S1). Keratins and highly abundant unspecific binders, which were also identified in control experiments by using blocked sepharose as an affinity matrix, were removed from the list. Among the remaining proteins we found more than 30 protein kinases, several oxidoreductases, ATP and GTP-binding enzymes, and nonprotein kinases. Additionally, we detected associated proteins (cyclins), which are known to interact with several of the identified protein kinases. Furthermore, the list contained more than 30 proteins, the majority of which are presumably unspecific binders because isoforms or other subunits of the same proteins or other members of the same protein families were found in control experiments as well. To obtain a comthan 90%, as expected, since CDKs are closely related and share a high level of amino acid sequence identity (40–70%).[40,41] In addition, six further kinases were inhibited by more than 90% (AURKA, CHEK1, MAPK8, MAPK9, STK3, and ST17A) and six by more than 80% (CAMK2D, CDK7, PRKD2, STK4, STK10, and ULK3). Because C1 inhibits protein kinases from several kinase families, we would expect an increasing number of highly inhibited targets by expanding the tested kinase panel to all available human protein kinases. Interestingly, not all kinases captured by the C1 matrix appeared to be highly inhibited in the assay panel. Five kinases were inhibited by 50–80% (CAMK2G, CHUK, FER, MAPK1, YES) and six (CDC42BPB, MAP2K1, PAK4, PKN2, PRKD3, RIPK2) by less than

50%; this indicates that the affinity capturing used in the setup in this study is not necessarily correlated with a high-affinity binding, but depends on both affinity and the expression level of the protein. Additionally, the protein extract used in this study might not accurately reflect the in vivo situation of intact cells with regard to the physicochemical behavior of the proteins. Furthermore, it has to be taken into consideration that some of the protein kinases initially identified in the pull-down approach by using the C1 matrix, do not bind to the inhibitor directly, but instead might be cocaptured by their association to a protein complex. Indeed, the identification of several cyclins, which are known to tightly interact with several of the identified CDKs, suggests that there are additional associated proteins. In particular, the protein kinases that show only a low inhibition by C1 (CDC42BPB, MAP2K1, PAK4, PKN2, PRKD3, RIPK2) might bind indirectly to the C1 matrix via other target proteins. These findings demonstrate that there is an essential need for the validation of the affinity of the compound to any protein captured by inhibitor pull-downs.

Application of a mimic to assess functional effects of the linker

Testing the mimic on the same panel of kinases revealed differences in the selectivity pattern compared to C1 (Figure 3). The mimic had less inhibitory potency against most of the tested kinases, which is very likely due to steric effects of the linker. However, we found a few examples against which the mimic was more active compared to C1 (CAMK2G, PAK4, PKN2, PRKD2). In these examples, the functional groups of the linker (e.g., the hydroxyl group) might form additional hydrogen bonds and thereby increase the binding affinity. Altogether, the effects of a linker are individual and depend on the structure of the respective binding pocket of a specific target. A mimic is useful to analyze these linker effects on a given target; this improves the data interpretation of chemical proteomics experiments, but it does not allow a general prediction of linker effects on target binding.

However, not only the linker but also the immobilization itself might affect the binding profile of the test compound. For instance, the immobilization itself might change the potency of the inhibitor. Additionally, a high local compound concentration on the bead surface might cause enhanced capturing of moderate binders present in high abundance, or cause steric effects that are difficult to predict. Whereas the coupling chemistry is well reflected by our design of the soluble mimic, the question of how the density of the inhibitor on the bead surface influences the binding pattern is barely addressed by testing the soluble mimic and is therefore difficult to quantify. Nevertheless, our findings on additional linker effects that influence the selectivity pattern of a compound are consistent with those recently reported by Saxena et al.[42] By employing different kinds of linkers for compound coupling in terms of drug target deconvolution, they found significantly different patterns of captured proteins. Both, their and our results demonstrate the need for a suitable assay to define the specificity of the interaction of a protein with the ligand under investigation.

Besides the investigation of the protein kinase binding profile of C1 with chemical proteomics, another focus of this study was the characterization of nonprotein kinase–compound interactions.

Characterization of the pyridoxal kinase–C1 interaction

Within our chemical proteomics approach, we identified the human pyridoxal kinase (PDXK) as being captured by the C1 matrix. Interestingly, PDXK was found to be targeted by the CDK2 inhibitor (*R*)-roscovitine, as well.[32] Surprisingly, the binding was shown to occur at the substrate binding site rather than at the ATP binding site, as demonstrated by cocrystallization experiments.[43] Contribution of PDXK binding to the biological activity of (*R*)-roscovitine was discussed, but found to be unlikely. However, PDXK was thought to trap (*R*)-roscovitine and thereby reduce the amount of inhibitor that is free to interact with its main targets.[33]

These findings prompted us to investigate the PDXK–C1 interaction in more detail. First, we performed serial affinity chromatography[44,45] to verify a specific enrichment of PDXK by the C1 matrix. We incubated HeLa cell extracts with the C1 matrix, and mixed the flow-through with a fresh C1 matrix. Specific binders were essentially captured by the first affinity matrix whereas the amounts of unspecifically bound proteins were similar for both matrices. Because PDXK was mainly retained by the first matrix, as demonstrated by immunodetection of PDXK, we concluded that specific binding of PDXK to the compound matrix had occurred (Figure S2).

We next addressed the question of whether the C1 matrix targets the ATP site or an alternative binding site of PDXK as shown for (*R*)-roscovitine. We employed sequential elution of C1 matrix using ATP, free C1–SL and LDS-SB to distinguish between capture with the ATP binding site from enrichment by alternative sites. We identified PDXK only in compound and LDS-SB elution fractions but not in the ATP fraction (Figure 4A, lanes 1–3). In parallel, the C1 matrix was sequentially eluted by using ATP, free (*R*)-roscovitine and LDS-SB. Interestingly, (*R*)-roscovitine was able to compete with immobilized C1 and eluted PDXK; this suggests a similar binding site for both compounds (Figure 4A, lanes 4–6). No PDXK enrichment and elution resulted with the control matrix (Figure 4A, lanes 7–9).

Based on the results with (*R*)-roscovitine, we assumed that C1 binds to PDXK at the pyridoxal binding site. Indeed, PDXK enrichment by the C1 matrix was reduced by competition when free pyridoxine (10 mM) was spiked into the cell extract, as shown by immunodetection of PDXK (Figure S3 in the Supporting Information). Due to these findings we generated a pyridoxal affinity matrix (Scheme 1) and applied a sequential elution scheme (ATP, pyridoxine, free C1–SL, and finally LDS-SB) to C1 matrix, pyridoxal matrix, and control matrix in parallel (Figure 4B). Because PDXK was eluted from both affinity matrices by pyridoxine and free C1–SL (and LDS-SB, Figure 4B, lanes 3–5), but not by ATP (Figure 4B, lane 2), we concluded

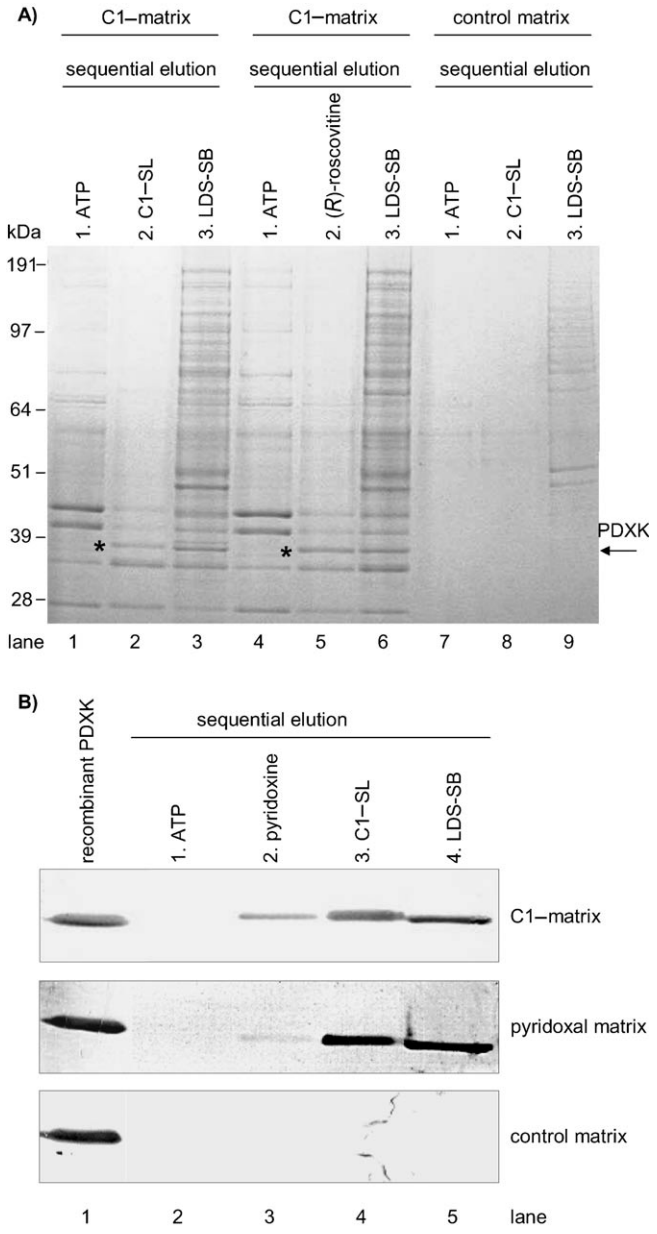

Figure 4. A) Pyridoxal kinase (PDXK) was found to bind to the C1 matrix by an alternative binding site and not the ATP binding site, similar to the PDXK–(*R*)-roscovitine interaction. After incubation with HeLa extracts and washing procedures, a sequential elution of C1 matrix was employed by using: 1) ATP (10 mM)/$MgCl_2$ (10 mM)/low-salt washing buffer; 2) a saturated C1–SL solution in low-salt washing buffer; 3) 2× LDS-SB/heat. Eluted proteins were loaded on SDS-PAGE and Coomassie stained. PDXK was identified in the compound and LDS-SB elution fractions, but not in the ATP fraction (asterisk); this suggests an alternative binding site rather than the ATP binding site (lanes 1–3). The same was observed when C1–SL was replaced by (*R*)-roscovitine, which is known to bind PDXK by its pyridoxal binding site (lanes 4–6). Because (*R*)-roscovitine was able to release PDXK from the C1 matrix, a similar PDXK binding site for C1 and (*R*)-roscovitine was concluded. PDXK was neither enriched nor eluted from the control matrix (lanes 7–9). B) PDXK was targeted by the C1 matrix at the pyridoxal binding site rather than the ATP binding site: C1 matrix, pyridoxal matrix and control matrix were loaded with HeLa extracts, washed and sequentially eluted by using: 1) ATP (10 mM)/$MgCl_2$ (10 mM)/low-salt washing buffer; 2) pyridoxine (10 mM)/low-salt washing buffer; 3) a saturated C1–SL solution in low-salt washing buffer; 4) 2× LDS-SB/heat. PDXK was eluted from both affinity matrices by pyridoxine and free C1–SL (immunodetection, lanes 3 and 4), but not by ATP (lane 1); this indicates that the PDXK–C1 interaction occurs at the substrate binding site rather than at the ATP binding site.

that the PDXK–C1 interaction occurs at the substrate binding site rather than at the ATP binding site.

After having demonstrated the enrichment of PDXK by the C1 matrix via the substrate binding site, we employed a PDXK activity assay to quantify the PDXK–C1 binding affinity. To this end, the activity of recombinant human PDXK was assayed in the presence of different concentrations of C1, C1–SL, mimic, and (*R*)-roscovitine. Even at the highest concentration tested (50 μM), a very modest inhibition of PDXK was found for (*R*)-roscovitine (Table 2, PDXK activity = (78 ± 13)% at 50 μM (*R*)-roscovitine); this confirms previously reported findings.[32] The same was true for C1 (50 μM, (92 ± 2)%), but an increasing linker length correlated with a more efficient decrease in PDXK activity (50 μM C1–SL: (81 ± 6)%, 50 μM mimic: (56 ± 7)%). We assume that additional interaction options provided by the linker contribute to the binding of the compound to the pyridoxal site (e.g., by hydrogen bonds or hydrophobic interactions). Nevertheless, the low-affinity binding of C1 and its analogues to PDXK was surprising to us. However, as it is suggested for the PDXK–(*R*)-roscovitine interaction, the high ATP concentration in the PDXK activity assay (2.5 mM) might have an influence on the activities measured by either reducing the affinity of PDXK for C1 or enhancing the affinity of PDXK for its substrate, pyridoxal. To determine the K_D of the compound for PDXK in the absence of ATP and of pyridoxal, we performed isothermal titration calorimetry (ITC); C1–SL was chosen for this experiment. A weak exothermal reaction was measured, but low binding heats prevented the exact K_D determination. However, the data suggest a K_D value of >10 μM, which is in agreement with our results from the PDXK activity assays (Figure S4). Thus, we assume that the significant enrichment of PDXK during chemical proteomics experiments can be explained by a combination of a high expression level of the ubiquitous PDXK, additional effects of the linking structure of the sepharose matrix, which contributes to the compound binding to the pyridoxal site, and a high local compound concentration on the bead surface. Altogether, it seems unlikely that effects caused by a PDXK–C1 interaction will play a role in pharmacological applications.

Table 2. The activity of native human PDXK was assayed[a] in the presence of C1, C1–SL, mimic (C1–LL) and (*R*)-roscovitine. Even at the highest concentration tested (50 μM), the C1 analogues showed only limited inhibition of PDXK activity. However, an increasing linker length caused stronger inhibition.

	C1	C1–SL	mimic	(*R*)-roscovitine	EDTA[c] (10 mM)
activity[b] [%]	92 ± 2	81 ± 6	56 ± 7	78 ± 13	11 ± 1

[a] Experiments were performed in triplicate; [b] as a percentage of vehicle control at 50 μM compound concentration; [c] negative control.

CA2 interaction revealed by an alternative immobilization route

Immobilization of C1 at the sulfonamide group is a suitable strategy for identifying targets that interact with the aminopyr-

imidine moiety (e.g., protein kinases). However, due to steric hindrance, interactions that occur at the benzenesulfonamide moiety of C1 are blocked with the C1 matrix. In fact, benzenesulfonamide moieties are known to inhibit most of the known carbonic anhydrase isozymes.[46] Especially the ubiquitously expressed cytosolic isoform carbonic anhydrase 2 (CA2)[47] is described to have a very high affinity for sulfonamides. To profile the C1 interactions more comprehensively, particularly with regard to CA2 binding, the analogue C1a was coupled to a solid support at the 4-position to give the C1a matrix (Scheme 1). C1a was also shown to inhibit CDK2 activity at low-nanomolar concentrations (Table 1, IC_{50} (CDK2/CycE) = 18 nM). Not being blocked by a linker at the benzenesulfonamide moiety, the C1a matrix was used for the identification of additional off-targets for our studied compound. Due to a lack of expression of CA2 in HeLa cells, H460 cells were included in this analysis. CA2 expression in H460 but not in HeLa cells was demonstrated by immunoblotting (Figure S5 in the Supporting Information). Indeed, CA2 was found to be enriched from H460 cell extracts by the C1a matrix by LC-MS/MS analysis of proteins unspecifically and specifically eluted with LDS-SB and free C1a (Figure S6 A), and this was validated by immunoblotting (Figure 5 A).

Commercially available human CA2 was used to determine the IC_{50} values for C1, C1–SL, mimic, and C1a. The IC_{50} values of C1 and C1a were in the submicromolar range (IC_{50} C1 = 331 nM, C1a = 995 nM for CA2), whereas C1–SL and the mimic had no inhibitory potential (Figure 5 B); this was most likely due to the steric hindrance that was caused by the linkers. The ubiquitous CA2 is involved in crucial physiological processes connected with respiration and transport of CO_2/bicarbonate, electrolyte secretion, bone resorption, calcification, etc.[46,48] Thus, binding of C1 to CA2 at submicromolar concentrations might cause unwanted biological effects of the compound or at least trap the compound and reduce the amount of free inhibitor that is available for on-target interaction. However, our findings show that the CA2–C1 interaction specifically occurs at the benzenesulfonamide moiety and that CA2 binding by the compound can easily be prevented by a small modification at the sulfonamide group. This structure–activity relationship information might help to improve the selectivity profile of the compound in the context of ongoing lead-optimization processes.

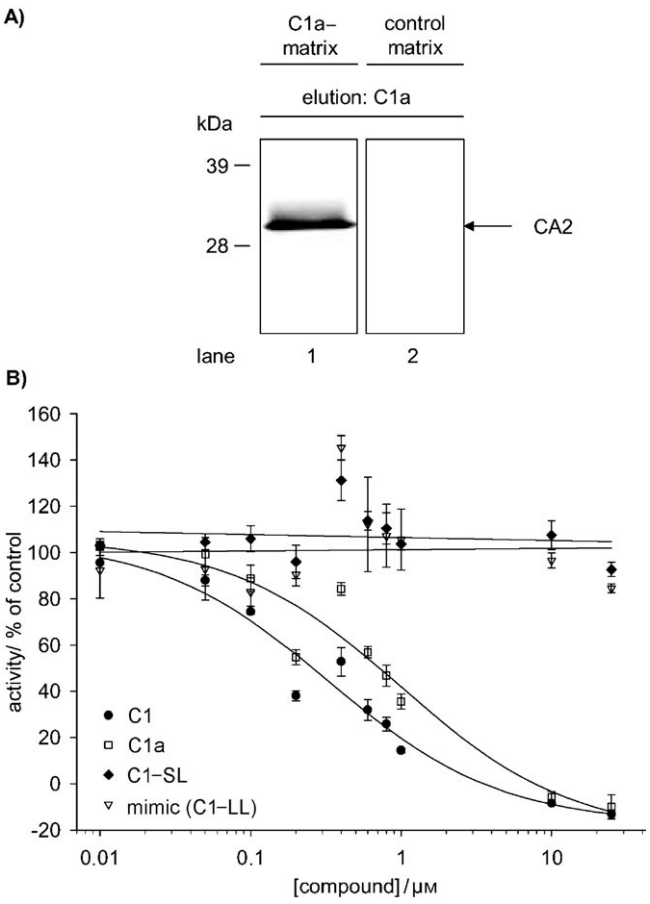

Figure 5. The C1 analogue, C1a, was immobilized by the aminopyrimidine moiety, and the corresponding C1a matrix was employed to investigate a potential interaction with CA2. A) Because the benzenesulfonamide moiety was not blocked by a linker, the C1a matrix captured CA2 from H460 extracts, as shown by immunodetection of specifically eluted CA2 from C1a matrix by using a saturated C1a solution in low-salt washing buffer (lane 1). No CA2 capturing resulted with the control matrix (lane 2). B) Inhibitory potentials of C1, C1–SL, mimic (C1–LL) and C1a on human CA2 activity were determined (IC_{50}). Medium affinity binding was found for C1 (IC_{50} = 331 nM) and C1a (IC_{50} = 995 nM), whereas C1–SL and the mimic had no inhibitory potential. These findings suggest that binding of CA2 to C1 can be prevented by a modification of the sulfonamide group of the compound.

The protein-binding profile of C1a matrix contained some protein kinases and revealed one further potential off-target: CMBL

Compared to the C1 matrix, a significantly lower amount of total protein was retained by the C1a matrix; this was demonstrated by a Coomassie stained SDS-PAGE of proteins that unspecifically eluted from the C1a matrix by using LDS-SB and heat (Figure S6 A). The overlap of two biological replicates by using the C1a matrix resulted in the identification of 37 proteins that fulfill the acceptance criteria (Table S2 in the Supporting Information). Keratins and unspecific binders that were also identified in control experiments by using control matrix and H460 protein extracts—in total 25 proteins—were not considered for further data interpretation.

We assume two major reasons for the lower total number of proteins retained by the C1a matrix compared to the C1 matrix. First, we expect that the ATP binding pocket of protein kinases and other purine-binding proteins is much less accessible by the C1a matrix. Thus, fewer specific interactions are expected to occur. Secondly, due to a lower number of directly interacting proteins, much less indirect capturing of proteins through association with other target proteins and protein complexes, or through unspecific hydrophobic interactions can occur.

Surprisingly, by employing the C1a matrix, we indeed identified some protein kinases (AURKA, CDK1, MAPK9) that were also captured by using the C1 matrix. This indicates that binding to the ATP binding pocket is not completely hampered with the C1a matrix. We assume that the entrance to the ATP

binding site is less size restricted with these kinases compared to the kinases found only with the C1 matrix. Because the linker arm of the matrix is flexible and can fold into the direction of the sulfonamide group, the immobilized compound might still be able to bind to the hinge region of the respective kinases. A very high inhibitory potency was found for C1 in the biochemical selectivity screen for these kinases (>90 for MAPK9 and even $>95\%$ for CDK1 and AURKA, Figure 3); therefore, the possibility that some of these kinases are cocaptured by binding to protein complexes appears to be very unlikely. However, because the C1a matrix was not optimized for capture of protein kinases, these findings were not investigated in more detail.

Eight proteins were exclusively identified by using the C1a matrix, including CA2 and the previously unknown potential off-target carboxymethylenebutenolidase homologue (CMBL, Figure S6A). Interestingly, CMBL was also identified by employing free C1a for specific elution of the proteins captured by the C1a matrix. Moreover, this protein was also identified by applying the C1a matrix and specific elution with HeLa cell extracts (Figure S6B). Because CMBL was not found by using the C1 matrix, we conclude that it binds to the sulfonamide moiety of the compound. This enzyme is described to have a hydrolase activity and is involved in detoxification pathways (KEGG pathways: 1,4-dichlorobenzene degradation 00627 and γ-hexachlorocyclohexane degradation 00361). The CMBL–compound interaction was not characterized in more detail for this study, but might be an object for further investigations of C1 profiling.

Conclusions

Here, we present an unbiased chemical proteomics approach for decoding nonprotein kinase off-targets of the multitarget protein kinase inhibitor, C1. We applied two different compound immobilization routes to identify off-targets interacting with distinct compound moieties. Furthermore, we employed a soluble mimic of the immobilized compound to confirm appropriate compound immobilization with regard to protein kinase capturing. After having captured several protein kinases by using the C1 matrix, we selected 27 kinases for a biochemical selectivity screen. A strong enzyme inhibition was found for the CDKs, as well as for several other kinases from different kinase families; this indicates the poor selectivity of the compound. Besides this, several kinases that were captured by the C1 matrix showed only a low inhibition in the selectivity studies. Thus, affinity capturing by the C1 matrix in the setup used in this study is not necessarily correlated with high-affinity binding, but depends on both affinity and expression levels. In addition, a protein extract might differ from the physiological conditions with regard to the physicochemical behavior of the proteins. Moreover, indirect capture of proteins by their association to other target proteins and protein complexes might occur. The low inhibitory potency ($<50\%$) of C1 toward some of the kinases initially identified by the affinity pull-down and the identification of cyclins, which are known to form complexes with CDKs, support this assumption. This underlines the essential need for additional methods, such as quantitative biochemical binding studies, to validate the results from affinity pull-down experiments.

Furthermore, we applied the mimic to assess the functional effects of the linker on target binding. For this purpose, the mimic was screened in the same panel of kinases that was used for the selectivity studies of C1. The comparison of the selectivity patterns of compound and mimic revealed various effects of the linker on distinct targets. Predominantly, the linker caused a reduction of inhibitory potential, which is very likely due to steric effects. However, some kinases showed increased inhibition by the mimic compared to C1; this was presumably due to additional interaction options provided by the linker. Thus, a mimic helps to improve data interpretation of chemical proteomics experiments, but it does not allow a general prediction of functional effects of the linker on target binding. Within our chemical proteomics approach, we found that the human pyridoxal kinase (PDXK) was captured by the C1 matrix. Interestingly, PDXK is described to also bind the CDK2 inhibitor, (*R*)-roscovitine. PDXK is a nonprotein kinase responsible for the phosphorylation of vitamin B6—a cofactor for numerous enzymes such as aminotransferases and decarboxylases. We demonstrated that the PDXK–C1 interaction occurs at the substrate binding site rather than at the ATP binding site. However, subsequent quantitative binding studies, which included several C1 analogues, revealed a very limited inhibition of PDXK activity. We conclude that it seems unlikely that effects observed in pharmacological applications could be caused by a PDXK–C1 interaction. By employing an alternative immobilization route for C1, we found carbonic anhydrase 2 (CA2) to be captured by the C1a matrix. Because the ubiquitous CA2 is inhibited by C1 in the submicromolar range (IC_{50}), as demonstrated by subsequent activity assays, unwanted pharmacological effects or a trapping of the compound due to this interaction have to be taken into consideration. However, our results indicate that a modification at the sulfonamide group prevents CA2 from binding, most likely due to steric hindrance.

To summarize, we introduced different compound immobilization routes as a valuable method for an unbiased off-target profiling by chemical proteomics. By successfully applying this methodology, we identified several off-targets that interact with distinct compound moieties. We propose to employ the strategy of different compound immobilization routes for the target identification of hit compounds that originate from phenotypic screens in cell-based assays or animal studies. Thus, we believe that the use of different immobilization routes will become a useful tool for future off-target and target-decoding strategies.

Experimental Section

Reagents and antibodies: Unless otherwise stated, all reagents were purchased from Sigma (Munich, Germany). Antibodies used were: monoclonal mouse anti-CDK2 antibody (Santa Cruz Biotechnology, Inc., Heidelberg, Germany), polyclonal rabbit anti-PDXK

(Abcam, plc., Cambridge, UK), and polyclonal rabbit anti-CA2 (Chemicon–Millipore, Billerica, MA, USA).

Compounds: C1, C1–SL, C1–LL and C1a were produced in-house. The correct compound identity was confirmed by ^{1}H NMR spectroscopy and MS.

C1: ^{1}H NMR ([D$_6$]DMSO): $\delta = 10.35$ (s, 1H), 8.23 (br s, 2H), 7.89 (m, 2H), 7.70 (m, 2H), 7.20 (br s, 2H), 4.12 (m, 2H), 3.19 ppm (br s, 1H); MS: *m/z* 383 (EI+).

C1–SL: ^{1}H NMR ([D$_6$]DMSO): $\delta = 9.87$ (s, 1H), 8.13 (s, 1H), 7.98 (m, 2H), 7.74 (br s, 2H), 7.61 (m, 4H), 4.11 (dd, 2H), 3.11 (t, 1H), 2.83 ppm (m, 4H); MS: *m/z* 425 (ESI+).

Mimic C1–LL: ^{1}H NMR ([D$_6$]DMSO): $\delta = 9.86$ (s, 1H), 8.43 (m, 2H), 8.12 (s, 1H), 7.99 (m, 2H), 7.61 (m, 4H), 4.11 (dd, 2H), 3.85 (m, 2H), 3.35 (m, 3H), 3.26 (m, 1H), 3.11 (t, 1H), 2.98 (m, 4H), 2.81 (m, 1H), 1.43 (m, 2H), 1.27 (m, 2H), 0.83 ppm (t, 3H); MS: *m/z* 555 (ESI+).

C1a: ^{1}H NMR ([D$_6$]DMSO): $\delta = 9.68$ (s, 1H), 8.12 (s, 1H), 7.75 (m, 6H), 7.20 (tr, 1H), 7.13 (s, 2H), 3.61 (m, 2H), 3.08 ppm (m, 2H); MS: *m/z* 387 (CI+).

Immobilization of diaminopyrimidines and control matrix: This was performed in a similar fashion to a previously described procedure.[49] Drained epoxy-activated Sepharose™ 6B (GE Healthcare Biosciences AB, Uppsala, Sweden) was resuspended in two volumes of either 20 mM C1–SL or C1a dissolved in coupling buffer (50% dimethylformamide/0.1 M Na_2CO_3, pH 11) and incubated, overnight, at room temperature in the dark. After being washed three times with coupling buffer, the remaining reactive groups were blocked with ethanolamine (1 M; pH 11). Subsequently, the washing steps were performed according to the manufacturer's instructions. The control matrix was prepared by directly blocking epoxy-activated Sepharose™ 6B with ethanolamine (1 M, pH 11), and further treated as described above. The matrixes were stored at 4 °C in the dark.

Immobilization of pyridoxal: Coupling of pyridoxal to EAH–Sepharose™ 4B (GE Healthcare Biosciences AB) was adapted from a previously described protocol.[50] The beads (50 mL) were pretreated as recommended by the manufacturer, and added to a pyridoxal hydrochloride solution (120 mM; 350 mL; pH 7). After being incubated, overnight, at room temperature in the dark, $NaBH_4$ (20 mg mL^{-1}) was added dropwise until all traces of yellow color had disappeared. Meanwhile, acetic acid (7%) was used to keep the pH below 9. Subsequently, the matrix was allowed to reach room temperature, and the pH was adjusted to 6 with acetic acid (7%) to destroy residual $NaBH_4$. After the pyridoxal matrix was washed with KCl solution (3 M; 250 mL) and H_2O (250 mL), the matrix was stored at 4 °C in the dark.

Cell culture and lysis: H460 cells (human large-cell lung carcinoma cell line, ATCC/LGC Standards GmbH, Wesel, Germany) were cultured in DMEM/Ham's F12 (1:1; Biochrom, Berlin, Germany) supplemented with fetal bovine serum (10%). Frozen HeLa cells (human cervix carcinoma cell line, CilBiotech, Mons, Belgium) and H460 cells were lysed in lysis buffer that contained Tris-HCl (50 mM), pH 8.0, NaCl (150 mM), glycerol (10%), NP-40 (0.5%), EGTA (1 mM), EDTA (1 mM), DTT (5 mM), orthovanadate (1 mM) and complete protease inhibitor cocktail (Roche Diagnostics GmbH, Mannheim, Germany). For affinity chromatography experiments, lysates were precleared by centrifugation (30 min, 50 000 *g*, 4 °C, Optima™ L-90K Ultracentrifuge, Beckmann Coulter, Krefeld, Germany) and the protein concentration was determined by using the Bradford method (Pierce Biotechnology, Rockford, IL, USA).

Affinity chromatography: Affinity chromatography experiments were performed as previously described.[49,51] HeLa and H460 cell extracts (~9 mg total protein, ~200 μL) were adjusted to 1 M NaCl. Optionally, pyridoxine (10 mM) in low-salt washing buffer (see below) was spiked into the sample. Cell extracts were incubated with drained affinity matrix (25 μL; C1–, C1a–, pyridoxal–matrix) or control matrix (50 μL) for 3 h at 4 °C in Micro Bio-Spin Chromatography Columns (Biorad, Hercules, CA, USA). Subsequently, the flow-through was discarded, but the beads were kept for the washing procedure. After three washing steps with high-salt washing buffer (450 μL; 1 M NaCl, 50 mM Tris-HCl, pH 8.0, 10% glycerol, 1 mM EGTA, 1 mM EDTA) and three steps with low-salt washing buffer (450 μL; 150 mM NaCl, otherwise the same composition as the high-salt washing buffer) the beads were (sequentially) eluted with several elution buffers (200 μL each, depending on the question addressed) for 20 min at 4 °C, or by LDS-SB elution buffer (22.5 μL) for 10 min at 90 °C. ATP buffer: ATP (10 mM), $MgCl_2$ (20 mM) in low-salt washing buffer; compound buffer: saturated compound solution in low-salt washing buffer; pyridoxine buffer: pyridoxine (10 mM) in low-salt washing buffer; LDS-SB: 2× LDS-sample buffer, 1× sample reducing agent (both from Invitrogen, Karlsruhe, Germany). The volume of the elution fractions, with the exception of LDS-SB elution fraction, which was directly loaded on SDS-PAGE,[52] was reduced to 100 μL by using a Speed Vac® Plus SC110A concentrator (GMI, Ramsey, MN, USA) before precipitation of proteins by using the 2D Clean-Up Kit (GE Healthcare Biosciences). Precipitated proteins were dissolved in LDS-SB (20 μL), and after reduction (1× sample reducing agent, 90 °C, 10 min) and alkylation (with 50 mM iodoacetamide, 30 min, room temperature, in the dark) were separated by 1D SDS-PAGE. Proteins were either transferred to a nitrocellulose membrane and immunoblotted with the indicated antibodies or stained with Coomassie and prepared for analysis by mass spectrometry.

Serial affinity chromatography: Cell extracts were treated as described above. The flow-through, however, was not discarded, but mixed with fresh affinity or control matrix and incubated for 3 h at 4 °C. After the washing and elution steps as described for affinity chromatography, samples were separated by SDS-PAGE and immunoblotted by using an anti-PDXK antibody.

LC-coupled mass spectrometry: Lanes from Coomassie stained SDS-PAGE gels were sliced across the separation range and subjected to in-gel tryptic digestion in a manner similar to a previously described procedure.[53] ESI-based LC-MS/MS analyses were carried out by using an Eksigent NanoLC 2D system (Eksigent, Dublin, CA, USA). A C18 capillary column (NanoSeparations, Nieuwkoop, Netherlands) with 5 μm biosphere material, 75 μm ID and 15 cm length was used at a flow rate of 250 nL min^{-1}. The samples were separated by a 35 min linear gradient of 2 to 35% acetonitrile in H_2O containing formic acid (0.1%). The HPLC was coupled to a quadrupole/time-of-flight mass spectrometer (QSTAR XL) by using a nanoelectrospray source (both from Applied Biosystems/MDS Sciex, Concord, Canada). The electrospray voltage was set to 2.0 kV. The data acquisition mode was set to one full MS scan (*m/z* range 300 to 1100) followed by three MS/MS events by using information-dependent acquisition (the three most intense ions from a given MS scan were subjected to CID). The peptide masses, which were selected for CID, were excluded from reanalysis for 30 s.

Data processing: The raw files from the QSTAR XL were converted to Mascot generic format-files by Mascot Daemon (version 2.2). MS/MS spectra were searched by using Mascot™ 2.0 software (Matrix Science Ltd., London, UK) against an in-house-curated version of the human IPI protein database combined with a decoy

version of this database,[54] which was created by a script supplied by Matrix Science. The search was performed with tryptic cleavage specificity with one missed cleavage site, a mass tolerance of 100 ppm for the precursor ions and 0.5 Da for the fragment ions, methionine oxidation, and cysteine carbamidomethylation as variable modifications. Protein identifications were accepted when at least two peptides with a Mascot ion score of ≥ 25 for each peptide were found. The false discovery rate (FDR) for peptides was $<5\%$ in each case. The protein redundancy in the dataset was eliminated by the ProteinScape software (version 1.3 SR2, Protagen/Bruker Daltonik GmbH, Bremen, Germany).[55] To further reduce dataset complexity by combining several splicing variants for one protein, and because gene IDs are more stable, BioXM software (version 2.5, BioMax Informatics AG, Martinsried, Germany) was used to replace IPI numbers by gene IDs as provided by the Entrez gene database. Resulting lists of gene IDs and gene products were used for further data analyses.

Expression of human PDXK: *E. coli* strain BL21 (DE3; Novagen, Madison, WI, USA) was transformed with the recombinant vector pET11a-PDXK, which was kindly provided by E. Leistner.[56] The recombinant strain BL21 (DE3)-pET11a-PDXK was grown in LB medium that contained ampicillin (200 $\mu g\,mL^{-1}$) at 37 °C until an OD_{600} of 1 was reached. Isopropyl thio-β-D-galactoside (IPTG) was added (final concentration of 0.01 mM) and the culture was incubated with shaking for 24 h. Protein expression was confirmed by SDS-PAGE. The cell pellet derived from 2 L of culture was frozen at −80 °C. The frozen bacteria were resuspended in ice-cold column buffer (100 mL; 50 mM Tris-HCl, pH 7.4; 200 mM NaCl, 1 mM EDTA) before microfluidizer (Microfluidics, Lampertheim, Germany) treatment. After sedimentation of the cell debris (45 min, 100000 *g*, 4 °C, Optima™ L-90K Ultracentrifuge) the supernatant was treated as described below.

Purification of PDXK: Cell-free protein extracts derived from 2 L of culture were adjusted to 100 mM KCl and subjected to affinity chromatography by using a pyridoxal matrix (preparation as described above) and size-exclusion chromatography as described previously.[50] The purity of the elution fractions as well as their protein concentrations were determined by LabChip® 90 (Caliper, Ruesselsheim, Germany).[57] In the final pool fraction, the identity of PDXK was verified by SDS-PAGE and LC-ESI-MS/MS.

Enzymatic assays

PDXK assay: The activity of recombinant human PDXK (without tag) was assayed in the presence of test compounds in a range of 1 nM–50 μM, as previously described.[56] The assay determines phosphorylation of pyridoxal by PDXK by measuring pyridoxal 5′-phosphate at its absorption maximum of 388 nm. Test compounds dissolved in DMSO were pipetted into the wells of a UV/vis-transparent 96-well microtiter plate (BD Biosciences Europe, Erembodegem, Belgium) that contained assay buffer (250 μL; 70 mM potassium phosphate, pH 6.2, 0.1 mM $ZnCl_2$, 2.5 mM ATP, 2.5 $\mu g\,mL^{-1}$ PDXK). The enzymatic reaction was started by the addition of substrate dissolved in H_2O (final pyridoxal concentration 0.5 mM). Absorbance was determined photometrically at 388 nm against a blank (same mixture of reagents but without enzyme) by using a SpectraMax 190 spectrophotometer (Molecular Devices, Sunnyvale, CA, USA) at 37 °C. The initial linear formation rate of pyridoxal 5′-phosphate was used to calculate PDXK activity; this was expressed as a percentage of vehicle control (wells that contained 2% DMSO without test compounds), which represented maximal activity. Curves were fitted to the averaged value of each triplicate by using Sigma Plot 8.02 (Systat Software GmbH, Erkrath, Germany). EDTA (10 mM) served as a negative control; DMSO (2%) was shown to have no effect on PDXK activity.

CA2 assay: The inhibitory potential of compounds on human CA2 activity was determined (IC_{50}). The assay determines the hydrolysis of 4-nitrophenyl acetate by carbonic anhydrases[58] by measuring 4-nitrophenolate at 400 nm. A Tecan Rainbow 96-well spectrophotometer (Tecan Group, Ltd., Maennedorf, Switzerland) was used for the measurements. Test compounds, which were dissolved in DMSO and covered a concentration range of 0.01–25 μM (final), were pipetted in triplicates into the wells of a 96-well microtiter ELISA plate. Wells containing solvent without test compound served as reference. Degassed assay buffer (10 mM Tris-HCl, pH 7.4, 80 mM NaCl) with CA2 (3 units per well) was added. The enzymatic reaction was started by the addition of substrate solution (1 mM 4-nitrophenyl acetate that was dissolved in H_2O-free acetonitrile; final substrate concentration 50 μM). The plate was incubated at room temperature for 60 min. Absorbance was determined photometrically at 400 nm against a blank (same mixture of reagents but without enzyme). The enzyme activity was expressed as a percentage of the vehicle control (2% DMSO without test compounds), which represented maximal activity.

CDK2/CycE assay: CDK2/CycE inhibitory activity of compounds was quantified by employing a CDK2/CycE HTRF® assay. Recombinant GST fusion proteins of human CDK2 and human CycE (ProQinase GmbH, Freiburg, Germany) were used to measure the phosphorylation of the biotinylated peptide biotin–Ttds-YISPLKSPYKISEG-amide (Jerini peptide technologies, Berlin, Germany). CDK2/CycE was incubated for 60 min at 22 °C in the presence of different concentrations of test compounds in assay buffer (5 μL; 50 mM Tris-HCl, pH 8.0, 10 mM $MgCl_2$, 1.0 mM dithiothreitol, 0.1 mM sodium orthovanadate, 10 μM ATP, 0.75 μM substrate, 0.01% (*v/v*) Nonidet-P40 (Sigma), 1% (*v/v*) DMSO). The concentration of CDK2/CycE was adjusted depending on the activity of the enzyme lot, and was chosen appropriately to measure the assay in the linear range. Typical concentrations were in the range of 1 $ng\,mL^{-1}$. The reaction was stopped by the addition of a solution of HTRF® detection reagents (5 μL; 0.2 μM streptavidine–XLent), Phospho-(Ser) CDKs substrate antibody (3.4 nM; product #2324B, Cell Signaling Technology, Danvers, MA, USA) and Prot-A-EuK (4 nM; Protein A labeled with europium cryptate from Cis Biointernational, France, product no. 61PRAKLB) in an aq. EDTA solution (100 mM EDTA, 800 mM KF, 0.2% (*w/v*) bovine serum albumin in 100 mM HEPES/NaOH, pH 7.0). The resulting mixture was incubated for 1 h at 22 °C to allow the formation of the complex between the phosphorylated biotinylated peptide and the detection reagents. Afterwards, the amount of phosphorylated substrate was evaluated by measurement of the resonance energy transfer from Prot-A-EuK to streptavidine–XLent. For this purpose, the fluorescence emissions at 620 and 665 nm after excitation at 350 nm were measured in a HTRF® reader, for example, a Rubystar (BMG Labtechnologies, Offenburg, Germany) or a Viewlux (Perkin–Elmer, Wiesbaden, Germany). The ratio of the emissions at 665 and 622 nm was taken as the measure for the amount of phosphorylated substrate. The data were normalized (enzyme reaction without inhibitor = 0% inhibition, all other assay components but no enzyme = 100% inhibition), and IC_{50} values were calculated by a four-parameter fit by using in-house software.

KinaseProfiler™ service: The inhibitory potential of C1 and the mimic (C1–LL) for selected kinases was screened by the KinaseProfiler™ Service provided by Upstate/Millipore (Dundee, UK) at 1 μM compound and 10 μM ATP. Detailed information and assay protocols are available under: http://www.millipore.com

Isothermal titration calorimetry: ITC experiments were performed by using a Microcal VP-ITC instrument (MicroCal, LLC, Northampton, MA, USA). The calorimeter was calibrated by using standard electrical pulses as recommended by the manufacturer. The sample cell was loaded with purified PDXK (12.6 μM) in potassium phosphate (0.1 M; pH 6.0). The syringe was loaded with C1–SL (140 μM) in the same buffer. To ensure the same buffer conditions, an aliquot of the size-exclusion chromatography buffer for protein purification was used to prepare the compound solution. Titrations were performed at 25 °C with injection volumes of 12 μL and a spacing of 300 s. Raw data were collected, corrected for ligand heats of dilution, and integrated by using the MicroCal Origin software supplied with the instrument.

Computational modeling: Based on cocrystallization experiments of CDK2 in complex with various C1 analogues,[39] C1 was modeled into the ATP binding pocket of CDK2 by using Discovery Studio 2.1 (Accelrys, Cambridge, UK). The solvent-accessible surface was calculated by using PyMOL (DeLano Scientific LLC, Palo Alto, CA, USA).

Acknowledgements

The authors thank K. Sauvageot, K. Burmeister, P. Rothhaupt for technical support, V. Pütter and J. Fanghänel for advice and help with the PDXK expression, purification, and the ITC experiments, M. Schäfer for preparing the computational model of the CDK2–C1 complex, A. Sommer for carefully reading the manuscript, and A. Becker for funding and support (all Bayer–Schering Pharma AG, Berlin, Germany). Special thanks are extended to E. Leistner (Institute for Pharmaceutical Biology, University of Bonn, Germany) for providing us with a recombinant vector of human PDXK and to E. Kirkness (Institute for Genomic Research, Rockville, MS, USA) for his agreement to use the vector.

Keywords: chemical proteomics · inhibitors · pyridoxal kinases · roscovitine · sulfonamides

[1] G. Manning, D. B. Whyte, R. Martinez, T. Hunter, S. Sudarsanam, *Science* **2002**, *298*, 1912–1934.
[2] P. Cohen, *Nat. Rev. Drug Discov.* **2002**, *1*, 309–315.
[3] J. S. Boehm, J. J. Zhao, J. Yao, S. Y. Kim, R. Firestein, I. F. Dunn, S. K. Sjostrom, L. A. Garraway, S. Weremowicz, A. L. Richardson, H. Greulich, C. J. Stewart, L. A. Mulvey, R. R. Shen, L. Ambrogio, T. Hirozane-Kishikawa, D. E. Hill, M. Vidal, M. Meyerson, J. K. Grenier, G. Hinkle, D. E. Root, T. M. Roberts, E. S. Lander, K. Polyak, W. C. Hahn, *Cell* **2007**, *129*, 1065–1079.
[4] J. D. Carpten, A. L. Faber, C. Horn, G. P. Donoho, S. L. Briggs, C. M. Robbins, G. Hostetter, S. Boguslawski, T. Y. Moses, S. Savage, M. Uhlik, A. Lin, J. Du, Y. W. Qian, D. J. Zeckner, G. Tucker-Kellogg, J. Touchman, K. Patel, S. Mousses, M. Bittner, R. Schevitz, M. H. Lai, K. L. Blanchard, J. E. Thomas, *Nature* **2007**, *448*, 439–444.
[5] H. Davies, G. R. Bignell, C. Cox, P. Stephens, S. Edkins, S. Clegg, J. Teague, H. Woffendin, M. J. Garnett, W. Bottomley, N. Davis, E. Dicks, R. Ewing, Y. Floyd, K. Gray, S. Hall, R. Hawes, J. Hughes, V. Kosmidou, A. Menzies, C. Mould, A. Parker, C. Stevens, S. Watt, S. Hooper, R. Wilson, H. Jayatilake, B. A. Gusterson, C. Cooper, J. Shipley, D. Hargrave, K. Pritchard-Jones, N. Maitland, G. Chenevix-Trench, G. J. Riggins, D. D. Bigner, G. Palmieri, A. Cossu, A. Flanagan, A. Nicholson, J. W. Ho, S. Y. Leung, S. T. Yuen, B. L. Weber, H. F. Seigler, T. L. Darrow, H. Paterson, R. Marais, C. J. Marshall, R. Wooster, M. R. Stratton, P. A. Futreal, *Nature* **2002**, *417*, 949–954.
[6] J. A. Engelman, K. Zejnullahu, T. Mitsudomi, Y. Song, C. Hyland, J. O. Park, N. Lindeman, C. M. Gale, X. Zhao, J. Christensen, T. Kosaka, A. J. Holmes, A. M. Rogers, F. Cappuzzo, T. Mok, C. Lee, B. E. Johnson, L. C. Cantley, P. A. Janne, *Science* **2007**, *316*, 1039–1043.
[7] M. Soda, Y. L. Choi, M. Enomoto, S. Takada, Y. Yamashita, S. Ishikawa, S. Fujiwara, H. Watanabe, K. Kurashina, H. Hatanaka, M. Bando, S. Ohno, Y. Ishikawa, H. Aburatani, T. Niki, Y. Sohara, Y. Sugiyama, H. Mano, *Nature* **2007**, *448*, 561–566.
[8] K. Strebhardt, A. Ullrich, *Nat. Rev. Cancer* **2006**, *6*, 321–330.
[9] A. N. Tse, R. Carvajal, G. K. Schwartz, *Clin. Cancer Res.* **2007**, *13*, 1955–1960.
[10] W. W. Smith, Z. Pei, H. Jiang, V. L. Dawson, T. M. Dawson, C. A. Ross, *Nat. Neurosci.* **2006**, *9*, 1231–1233.
[11] M. L. Hayashi, B. S. Rao, J. S. Seo, H. S. Choi, B. M. Dolan, S. Y. Choi, S. Chattarji, S. Tonegawa, *Proc. Natl. Acad. Sci. USA* **2007**, *104*, 11489–11494.
[12] K. A. Whartenby, P. A. Calabresi, E. McCadden, B. Nguyen, D. Kardian, T. Wang, C. Mosse, D. M. Pardoll, D. Small, *Proc. Natl. Acad. Sci. USA* **2005**, *102*, 16741–16746.
[13] P. S. Changelian, M. E. Flanagan, D. J. Ball, C. R. Kent, K. S. Magnuson, W. H. Martin, B. J. Rizzuti, P. S. Sawyer, B. D. Perry, W. H. Brissette, S. P. McCurdy, E. M. Kudlacz, M. J. Conklyn, E. A. Elliott, E. R. Koslov, M. B. Fisher, T. J. Strelevitz, K. Yoon, D. A. Whipple, J. Sun, M. J. Munchhof, J. L. Doty, J. M. Casavant, T. A. Blumenkopf, M. Hines, M. F. Brown, B. M. Lillie, C. Subramanyam, C. Shang-Poa, A. J. Milici, G. E. Beckius, J. D. Moyer, C. Su, T. G. Woodworth, A. S. Gaweco, C. R. Beals, B. H. Littman, D. A. Fisher, J. F. Smith, P. Zagouras, G. A. Magna, M. J. Saltarelli, K. S. Johnson, L. F. Nelms, S. G. Des Etages, L. S. Hayes, T. T. Kawabata, D. Finco-Kent, D. L. Baker, M. Larson, M. S. Si, R. Paniagua, J. Higgins, B. Holm, B. Reitz, Y. J. Zhou, R. E. Morris, J. J. O'Shea, D. C. Borie, *Science* **2003**, *302*, 875–878.
[14] L. Buckbinder, D. T. Crawford, H. Qi, H. Z. Ke, L. M. Olson, K. R. Long, P. C. Bonnette, A. P. Baumann, J. E. Hambor, W. A. Grasser, III, L. C. Pan, T. A. Owen, M. J. Luzzio, C. A. Hulford, D. F. Gebhard, V. M. Paralkar, H. A. Simmons, J. C. Kath, W. G. Roberts, S. L. Smock, A. Guzman-Perez, T. A. Brown, M. Li, *Proc. Natl. Acad. Sci. USA* **2007**, *104*, 10619–10624.
[15] G. Solinas, C. Vilcu, J. G. Neels, G. K. Bandyopadhyay, J. L. Luo, W. Naugler, S. Grivennikov, A. Wynshaw-Boris, M. Scadeng, J. M. Olefsky, M. Karin, *Cell Metab.* **2007**, *6*, 386–397.
[16] R. Capdeville, E. Buchdunger, J. Zimmermann, A. Matter, *Nat. Rev. Drug Discov.* **2002**, *1*, 493–502.
[17] T. Morwick, A. Berry, J. Brickwood, M. Cardozo, K. Catron, M. DeTuri, J. Emeigh, C. Homon, M. Hrapchak, S. Jacober, S. Jakes, P. Kaplita, T. A. Kelly, J. Ksiazek, M. Liuzzi, R. Magolda, C. Mao, D. Marshall, D. McNeil, A. Prokopowicz, III, C. Sarko, E. Scouten, C. Sledziona, S. Sun, J. Watrous, J. P. Wu, C. L. Cywin, *J. Med. Chem.* **2006**, *49*, 2898–2908.
[18] P. Pevarello, M. G. Brasca, R. Amici, P. Orsini, G. Traquandi, L. Corti, C. Piutti, P. Sansonna, M. Villa, B. S. Pierce, M. Pulici, P. Giordano, K. Martina, E. L. Fritzen, R. A. Nugent, E. Casale, A. Cameron, M. Ciomei, F. Roletto, A. Isacchi, G. Fogliatto, E. Pesenti, W. Pastori, A. Marsiglio, K. L. Leach, P. M. Clare, F. Fiorentini, M. Varasi, A. Vulpetti, M. A. Warpehoski, *J. Med. Chem.* **2004**, *47*, 3367–3380.
[19] M. Wittman, J. Carboni, R. Attar, B. Balasubramanian, P. Balimane, P. Brassil, F. Beaulieu, C. Chang, W. Clarke, J. Dell, J. Eummer, D. Frennesson, M. Gottardis, A. Greer, S. Hansel, W. Hurlburt, B. Jacobson, S. Krishnananthan, F. Y. Lee, A. Li, T. A. Lin, P. Liu, C. Ouellet, X. Sang, M. G. Saulnier, K. Stoffan, Y. Sun, U. Velaparthi, H. Wong, Z. Yang, K. Zimmermann, M. Zoeckler, D. Vyas, *J. Med. Chem.* **2005**, *48*, 5639–5643.
[20] M. Bantscheff, D. Eberhard, Y. Abraham, S. Bastuck, M. Boesche, S. Hobson, T. Mathieson, J. Perrin, M. Raida, C. Rau, V. Reader, G. Sweetman, A. Bauer, T. Bouwmeester, C. Hopf, U. Kruse, G. Neubauer, N. Ramsden, J. Rick, B. Kuster, G. Drewes, *Nat. Biotechnol.* **2007**, *25*, 1035–1044.
[21] S. E. Hall, *Drug Discovery Today* **2006**, *11*, 495–502.
[22] R. Morphy, C. Kay, Z. Rankovic, *Drug Discovery Today* **2004**, *9*, 641–651.
[23] A. Budillon, F. Bruzzese, E. Di Gennaro, M. Caraglia, *Curr. Drug Targets* **2005**, *6*, 337–351.
[24] J. Verweij, M. de Jonge, *J. Clin. Oncol.* **2007**, *25*, 2340–2342.
[25] H. Daub, *Biochim. Biophys. Acta Proteins Proteomics* **2005**, *1754*, 183–190.
[26] C. Hopf, M. Bantscheff, G. Drewes, *Neurodegener. Dis.* **2007**, *4*, 270–280.
[27] H. Katayama, Y. Oda, *J. Chromatogr. B* **2007**, *855*, 21–27.
[28] M. Knockaert, L. Meijer, *Biochem. Pharmacol.* **2002**, *64*, 819–825.

[29] U. Kruse, M. Bantscheff, G. Drewes, C. Hopf, *Mol. Cell. Proteomics* **2008**, *7*, 1887–1901.
[30] S. J. McClue, D. Blake, R. Clarke, A. Cowan, L. Cummings, P. M. Fischer, M. MacKenzie, J. Melville, K. Stewart, S. Wang, N. Zhelev, D. Zheleva, D. P. Lane, *Int. J. Cancer* **2002**, *102*, 463–468.
[31] S. de La Motte, A. Gianella-Borradori, *Int. J. Clin. Pharmacol. Ther.* **2004**, *42*, 232–239.
[32] S. Bach, M. Knockaert, J. Reinhardt, O. Lozach, S. Schmitt, B. Baratte, M. Koken, S. P. Coburn, L. Tang, T. Jiang, D. C. Liang, H. Galons, J. F. Dierick, L. A. Pinna, F. Meggio, F. Totzke, C. Schachtele, A. S. Lerman, A. Carnero, Y. Wan, N. Gray, L. Meijer, *J. Biol. Chem.* **2005**, *280*, 31208–31219.
[33] K. Bettayeb, H. Sallam, Y. Ferandin, F. Popowycz, G. Fournet, M. Hassan, A. Echalier, P. Bernard, J. Endicott, B. Joseph, L. Meijer, *Mol. Cancer Ther.* **2008**, *7*, 2713–2724.
[34] J. A. Kerry, M. Rohde, F. Kwok, *Eur. J. Biochem.* **1986**, *158*, 581–585.
[35] R. Percudani, A. Peracchi, *EMBO Rep.* **2003**, *4*, 850–854.
[36] A. C. Eliot, J. F. Kirsch, *Annu. Rev. Biochem.* **2004**, *73*, 383–415.
[37] F. Gachon, P. Fonjallaz, F. Damiola, P. Gos, T. Kodama, J. Zakany, D. Duboule, B. Petit, M. Tafti, U. Schibler, *Genes Dev.* **2004**, *18*, 1397–1412.
[38] K. Wada, S. Ishigaki, K. Ueda, M. Sakata, M. Haga, *Chem. Pharm. Bull.* **1985**, *33*, 3555–3557.
[39] U. Lücking, G. Siemeister, M. Schaefer, H. Briem, M. Krueger, P. Lienau, R. Jautelat, *ChemMedChem* **2007**, *2*, 63–77.
[40] D. O. Morgan, *Nature* **1995**, *374*, 131–134.
[41] K. T. Chin, S. Y. Ohki, D. Tang, H. C. Cheng, J. H. Wang, M. Zhang, *J. Biol. Chem.* **1999**, *274*, 7120–7127.
[42] C. Saxena, E. Zhen, R. E. Higgs, J. E. Hale, *J. Proteome Res.* **2008**, *7*, 3490–3497.
[43] L. Tang, M. H. Li, P. Cao, F. Wang, W. R. Chang, S. Bach, J. Reinhardt, Y. Ferandin, H. Galons, Y. Wan, N. Gray, L. Meijer, T. Jiang, D. C. Liang, *J. Biol. Chem.* **2005**, *280*, 31220–31229.
[44] G. C. Terstappen, C. Schlupen, R. Raggiaschi, G. Gaviraghi, *Nat. Rev. Drug Discovery* **2007**, *6*, 891–903.
[45] K. Yamamoto, A. Yamazaki, M. Takeuchi, A. Tanaka, *Anal. Biochem.* **2006**, *352*, 15–23.
[46] C. T. Supuran, A. Scozzafava, *Bioorg. Med. Chem.* **2007**, *15*, 4336–4350.
[47] L. Puccetti, G. Fasolis, A. Cecchi, J. Y. Winum, A. Gamberi, J. L. Montero, A. Scozzafava, C. T. Supuran, *Bioorg. Med. Chem. Lett.* **2005**, *15*, 2359–2364.
[48] A. Thiry, C. T. Supuran, B. Masereel, M. Jean, *J. Med. Chem.* **2008**, *51*, 3051–3056.
[49] K. Godl, J. Wissing, A. Kurtenbach, P. Habenberger, S. Blencke, H. Gutbrod, K. Salassidis, M. Stein-Gerlach, A. Missio, M. Cotten, H. Daub, *Proc. Natl. Acad. Sci. USA* **2003**, *100*, 15434–15439.
[50] C. D. Cash, M. Maitre, J. F. Rumigny, P. Mandel, *Biochem. Biophys. Res. Commun.* **1980**, *96*, 1755–1760.
[51] D. Brehmer, K. Godl, B. Zech, J. Wissing, H. Daub, *Mol. Cell. Proteomics* **2004**, *3*, 490–500.
[52] U. K. Laemmli, *Nature* **1970**, *227*, 680–685.
[53] A. Shevchenko, H. Tomas, J. Havlis, J. V. Olsen, M. Mann, *Nat. Protoc.* **2007**, *1*, 2856–2860.
[54] J. E. Elias, W. Haas, B. K. Faherty, S. P. Gygi, *Nat. Methods* **2005**, *2*, 667–675.
[55] M. Blüggel, S. Bailey, G. Korting, C. Stephan, K. A. Reidegeld, H. Thiele, R. Apweiler, M. Hamacher, H. E. Meyer, *Proteomics* **2004**, *4*, 2361–2362.
[56] U. Kästner, C. Hallmen, M. Wiese, E. Leistner, C. Drewke, *FEBS J.* **2007**, *274*, 1036–1045.
[57] S. Lin, A. S. Fischl, X. Bi, W. Parce, *Anal. Biochem.* **2003**, *314*, 97–107.
[58] Y. Pocker, J. T. Stone, *Biochemistry* **1967**, *6*, 668–678.

Received: December 1, 2008
Published online on April 6, 2009

